Quaternary International 455 (2017) 82–92

Contents lists available at ScienceDirect

Quaternary International

journal homepage: www.elsevier.com/locate/quaint

Topographic controls on the debris-cover extent of glaciers in the Eastern Himalayas: Regional analysis using a novel high-resolution glacier inventory

Sunal Ojha [a], Koji Fujita [a, *], Akiko Sakai [a], Hiroto Nagai [b], Damodar Lamsal [a, c]

[a] Graduate School of Environmental Studies, Nagoya University, Chikusa-ku, Nagoya, 464-8601, Japan
[b] Earth Observation Research Center, Japan Aerospace Exploration Agency, Tsukuba, Ibaraki, 305-8505, Japan
[c] Asia Air Survey Co., Ltd., Kanagawa, 215-0004, Japan

A R T I C L E I N F O

Article history:
Received 26 November 2016
Received in revised form
14 July 2017
Accepted 4 August 2017
Available online 10 August 2017

A B S T R A C T

To better understand the influence of topography on the formation of Himalayan debris-covered glaciers, we manually digitized 5301 glaciers, covering an area of 5691 ± 893 km^2, from high-resolution Advanced Land Observing Satellite imagery, and identified 842 debris-covered glaciers with a debris-covered area of 3839 ± 753 km^2. This estimation of the debris-covered area of these glaciers is a novel approach in the Eastern Himalayas. We investigated the relationship between the debris-covered area and the corresponding potential debris supply (PDS) slopes for the debris-covered glaciers across the region. The PDS slopes on the southern side show better correlation with their debris-covered area formation than those situated on the northern side of the Himalayan barrier, with this correlation weakening toward the western massifs. Further investigation showed that PDS slopes oriented SE to W exert a stronger control on the formation of debris-covered areas, which is related to the diurnal freeze–thaw cycle on the southern slope of the mountain barrier.

1. Introduction

Himalayan glaciers play a crucial role in the maintenance of regional water resources in South Asia (Immerzeel et al., 2013); however, their response to climate change varies spatially (Fujita and Nuimura, 2011; Yao et al., 2012; Cogley, 2016), making accurate assessments of their ongoing and future contributions to water resources difficult. Limited accessibility, primarily due to the rugged terrain and poor socioeconomic conditions, hinder in situ observations in the high mountains, as previous researchers typically relied on the limited number of glaciers located at relatively lower elevations (Tshering and Fujita, 2016). Never-the-less, heterogeneous fluctuations in the mass balance of Himalayan glaciers have been gradually and increasingly revealed by in situ observations (Fujita and Nuimura, 2011; Yao et al., 2012; Zemp et al., 2015; Tshering and Fujita, 2016), remote sensing measurements (Bolch et al., 2012; Kääb et al., 2012; Nuimura et al., 2012, 2017; Gardelle et al., 2013; Ragettli et al., 2016), and numerical modeling (Fujita, 2008; Fujita and Nuimura, 2011; Shea et al., 2015).

A glacier inventory is a basic dataset used in glaciological investigations such as monitoring, modeling, and regional climatic analysis (e.g., Kääb et al., 2012; Gardelle et al., 2013; Sakai et al., 2015). Multiple glacier inventories have been created recently for the high mountains of Asia, including the Randolph Glacier Inventory (RGI: Pfeffer et al., 2014), International Centre for Integrated Mountain Development (ICIMOD, IGI hereafter: Bajracharya et al., 2014a), Glacier Area Mapping for Discharge from the Asian Mountains (GAMDAM, GGI hereafter: Nuimura et al., 2015), and the 2nd Chinese Glacier Inventory (CGI: Guo et al., 2015). However, these various inventories contain discrepancies in terms of the number of glaciers inventoried and their associated areal coverage (Nagai et al., 2016), which may lead to inaccurate regional estimates of water storage across the Himalayas. All of the above-mentioned inventories are based on the relatively coarse-resolution Landsat satellite images (30 m), which do not capture some of the smaller glaciers that are susceptible to disappearing in response to recent climate change (Paul et al., 2013; Ojha et al., 2016).

The contribution of debris cover to the overall evolution of debris-covered glaciers in the Himalayan region is poorly understood (Scherler et al., 2011a; Fujita and Sakai, 2014). The ablation

* Corresponding author.
E-mail address: cozy@nagoya-u.jp (K. Fujita).

http://dx.doi.org/10.1016/j.quaint.2017.08.007
1040-6182/

zone of most of the glaciers in this region is covered with a debris mantle. Because of the insulating properties of the debris, glaciers covered with a thick debris mantle tend to melt more slowly than those with only a thin debris mantle (Mattson et al., 1993). However, remote sensing analysis suggests comparable surface lowering rates for both debris-covered and debris-free glaciers (Kääb et al., 2012; Nuimura et al., 2012). In the high mountains of Asia, Scherler et al. (2011b) reported that glaciers situated at lower relief zones were primarily nourished by snowfall and thus had little or no debris cover, whereas those having steep accumulation zones had thick debris mantle. In the Bhutan Himalaya, Nagai et al. (2013) found that the south-facing, ice-free head walls above glaciers were the primary contributors to formation of debris-covered area through diurnal freeze–thaw cycles. However, previous studies in the Eastern Himalayas have scarcely dealt with debris-covered areas and their regional features, and the formation of debris-covered areas to local topography has rarely been addressed at the regional scale. This study thus aims to investigate the relationship between topographic settings and the extent of the debris-covered area in the Eastern Himalayas using a newly created high-resolution glacier inventory.

2. Study area, data, and methods

2.1. Study area

We studied both debris-free (hereafter termed the C-glacier, in reference to a clean-type glacier) and debris-covered (hereafter termed the D-glacier) glaciers and their spatial distribution across the Eastern Himalayas (85.0–92.0°E; 27.5–29.0°N) on both sides of the Himalayan barrier, and covering the political territories of Bhutan, India, China, and Nepal (Fig. 1a). Glaciers in the region form at high elevations, ranging from 4000 to 7600 m above sea level (a.s.l) (Bajracharya et al., 2014a), and have been rapidly shrinking over recent decades (Gardelle et al., 2013; Ojha et al., 2016). We divided our study area into four massifs: namely Langtang (LT), Khumbu (KB), Kanchenjunga-Sikkim (KS), and Bhutan (BT). We further categorized the glaciers into southern slope (hereafter termed S-glacier) and northern slope (hereafter termed N-glacier) glaciers, in which the Eastern Himalayas mountain barrier is viewed as a climatic barrier, to understand the role of large mountain ranges in the formation of debris cover on glaciers. This geographical separation closely follows the political boundaries of the neighboring nations, barring a few areas in the western massifs (Fig. 1b).

2.2. ALOS imagery

We created a new glacier inventory for the Eastern Himalayas using images taken by the Panchromatic Remote-sensing Instrument for Stereo Mapping (PRISM, 2.5-m resolution) and Advanced Visible and Near Infrared Radiometer type 2 (AVNIR-2, 10-m resolution), both of which are on board the Advanced Land Observing Satellite (ALOS). All of the PRISM images used in this study were acquired between 2006 and 2011, mostly during the post-monsoon season. In total, 104 (out of 1536 available images) PRISM images and 4 (out of 23 available images) AVNIR-2 images, possessing minimal cloud and snow cover, were selected for glacier delineation. Most of the glaciers (>99%) were delineated from the PRISM images, whereas AVNIR-2 images were used only in those areas where the PRISM images were unavailable. Most of the images (97) were orthorectified using PRISM-derived digital elevation models

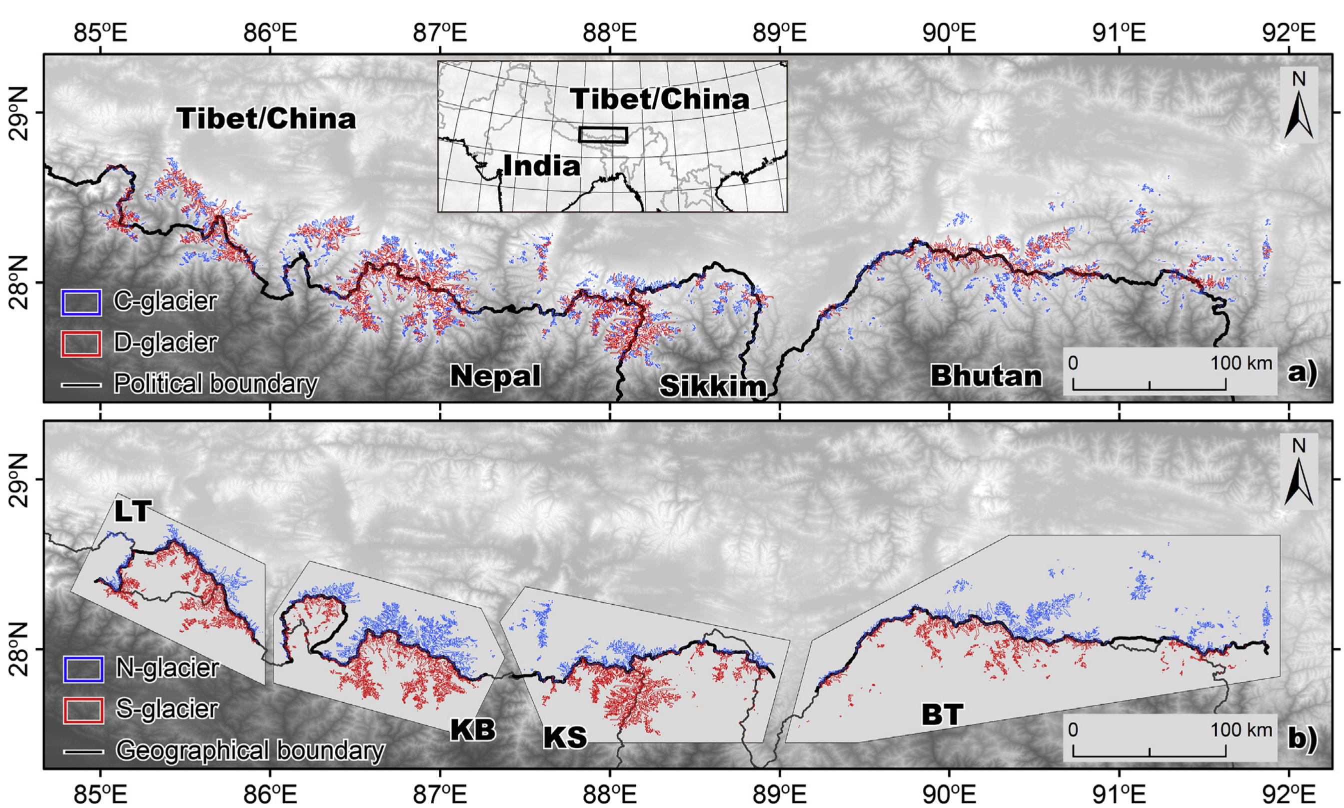

Fig. 1. Spatial distributions of: (a) extent of debris-free (C-glacier) and debris-covered (D-glacier) glaciers across the Eastern Himalayas, and (b) extent of northern-side (N-glacier) and southern-side (S-glacier) glaciers, which are distinguished by the geographical boundary of the Eastern Himalaya mountain barrier. Regional statistics are analyzed for the Langtang (LT), Khumbu (KB), Kanchenjunga-Sikkim (KS), and Bhutan (BT) massifs, whose areas are defined by the light gray polygons.

(DEMs) created using the Digital Surface Model and Ortho-image Generation Software for ALOS PRISM (DOGS-AP: Takaku and Tadano, 2009), with the remaining seven images orthorectified using the Leica Photogrammetric Suite (LPS 2011), as per the procedures adopted for Bhutan (Nagai et al., 2013, 2016) and Nepal (Ojha et al., 2016).

The second version of the Global Digital Elevation Model produced from the Advanced Spaceborne Thermal Emission and Reflection Radiometer (ASTER-GDEM2; 1-arcsec, approximately 30-m resolution; Tachikawa et al., 2011), was used for the generation of contour maps, slope maps, and other topographic parameters. This is because the PRISM-DEMs contain numerous voids in the upper accumulation area where the snow surface lacks sufficient contrast to create stereo views, whereas those voids are filled by multiple DEMs in the ASTER-GDEM2. The ASTER-GDEM2 is also more accurate than the Shuttle Radar Topography Mission (SRTM) where high and steep mountains are concerned (Luedeling et al., 2007; Reuter et al., 2007; Nuimura et al., 2015).

2.3. Glacier delineation

Glacier delineation of the high mountains in Asia is a challenging task because no single methodology is able to reflect the real ground conditions over an entire region. Existing delineation methodologies depend largely on the type of glacier, the extent of the study area, the type of imagery used, the quality of the images used (e.g., season of image acquisition and snow cover conditions), and the intended accuracy (Paul et al., 2013; Cogley, 2016). For instance, the global and regional inventories, such as the RGI (Pfeffer et al., 2014) and IGI (Bajracharya et al., 2014a, 2014b), are based on semi-automatic delineation, whereas the GGI (Nuimura et al., 2015), which covers the high mountains in Asia, is based completely on manual digitization. Although semi-automatic delineation offers high accuracy (ranging between 2% and 3% in area) and is reproducible for debris-free glaciers, it requires manual correction where debris-covered glaciers exist (Paul et al., 2013). As our study region is abundantly populated with debris-covered glaciers, we preferred the manual approach, as this was the same method successfully applied for the GGI (Nuimura et al., 2015), as well as regional glacier inventories in Bhutan (Nagai et al., 2013, 2016) and eastern Nepal (Ojha et al., 2016).

Glaciers were identified according to the guidelines outlined by the Global Land Ice Measurements from Space (GLIMS) initiative (Racoviteanu et al., 2009; Raup and Khalsa, 2010), which recommends that a single operator and the same resolution images are used throughout the delineation process to reduce ambiguities among the different operators and image resolutions. The boundary and its surrounding areas are discriminated by observing multiple ALOS images taken on different dates to avoid misinterpretation caused by seasonal snow cover (Nagai et al., 2013, 2016). Slope distribution and contour lines generated from the ASTER-GDEM2 help to distinguish the upper boundaries of the glaciers, whereas snowfields are separated from the glacier surface by interpreting the surface roughness visually from multiple images. In addition, ice cover above the bergschrund and glacier on steep slopes is also considered part of the glacier surface, as per the GLIMS tutorial (Raup and Khalsa, 2010). Finally, the delineated glacier outlines are overlain on high-resolution Google Earth images for further improvement and correction. All the procedures implemented here were also carried out for glacier delineation across the Bhutan and Nepal Himalayas (Nagai et al., 2013, 2016; Ojha et al., 2016).

To understand how climatic influences and geographical settings shape glacier distribution, we categorized each glacier as either a C- or D-glacier, and further separated the D-glaciers into their debris-free (hereafter termed the C-part) and debris-covered parts (hereafter termed the D-part). Although the identification was rather subjective, the upper boundaries of the D-part areas were confirmed by inspecting multiple images from different dates over the same season. The polygons were later improved with the help of high-resolution Google Earth images.

2.4. Potential debris supply slope

The concept of the potential debris supply (PDS) slope was proposed to understand the formation of debris-covered glaciers in the Bhutan Himalaya (Nagai et al., 2013). The PDS slope is defined as the slope that could supply a debris mantle onto the glacier surface via rockfalls or avalanches, and was manually digitized as a continuous slope between the glacier boundary and mountain crest (Fig. 2). Mountain ridges were confirmed by contour and slope maps generated from the ASTER-GDEM2 data. Slopes interrupted by hills or lateral moraines were excluded from the PDS slopes, as the debris from these slopes is prevented from reaching the glacier surface by local depressions, whereas the slopes of lateral moraines were included if they are inclined toward the glacier surface. Small depressions (<60 m in size) that were not identifiable from the contour map were manually corrected with the help of high-resolution Google Earth images and excluded from the PDS area. Furthermore, the polygons were compared with the Google Earth images as a quality check. As the PDS slopes tend to be steep, the PDS slope area was divided by the cosine of its respective slope gradient to estimate its true area.

2.5. Accuracy of delineated glacier

The accuracy of the delineated glacier outlines depends largely upon the pixel resolution, image quality, threshold value, and operator experience (Paul et al., 2013). However, different approaches to accuracy estimation have been proposed by different authors, dependent on their requirements and intended study focus (Fujita et al., 2009; Bajracharya et al., 2014a, 2014b). The methodology proposed by Nagai et al. (2016) in the Bhutan Himalaya was based on multiple digitizations of debris-free and debris-covered glaciers, in which they digitized 10 debris-free glaciers and 6 debris-covered glaciers using four different operators, and an uncertainty ratio was calculated based on the mean and standard deviation of these digitized areas. In the Bhutan Himalaya, larger uncertainties were found for smaller glaciers and vice versa, regardless of the degree of debris cover. As our study area is similar to that of the Bhutan Himalaya, in terms of glacier formation and physiographic characteristics, we opted for the methodology proposed by Nagai et al. (2016), which is based on two different empirical equations: $y = 30.5x^{-0.19}$ for C-glaciers and $y = 7.54x^{-0.12}$ for D-glaciers, where x and y denote the area of a given glacier and its associated uncertainty, respectively.

3. Results and discussion

3.1. ALOS-derived glacier inventory (AGI)

We identified 5301 glaciers across our study area, covering a total area of 5691 ± 893 km^2, and they comprised 4459 C-glaciers covering an area of 1853 ± 141 km^2 (0.42 km^2 per glacier) and 842 D-glaciers covering an area of 3839 ± 753 km^2 (4.6 km^2 per glacier: Table 1 and Fig. 1a). Our ALOS-derived glacier inventory (AGI) covers 6%, in terms of both number and area, of the GGI, which covers all of the high mountains in Asia (Nuimura et al., 2015). The number-to-area distribution of C-glaciers identified in this study is heavily right-skewed, supporting highlighting the proliferation of

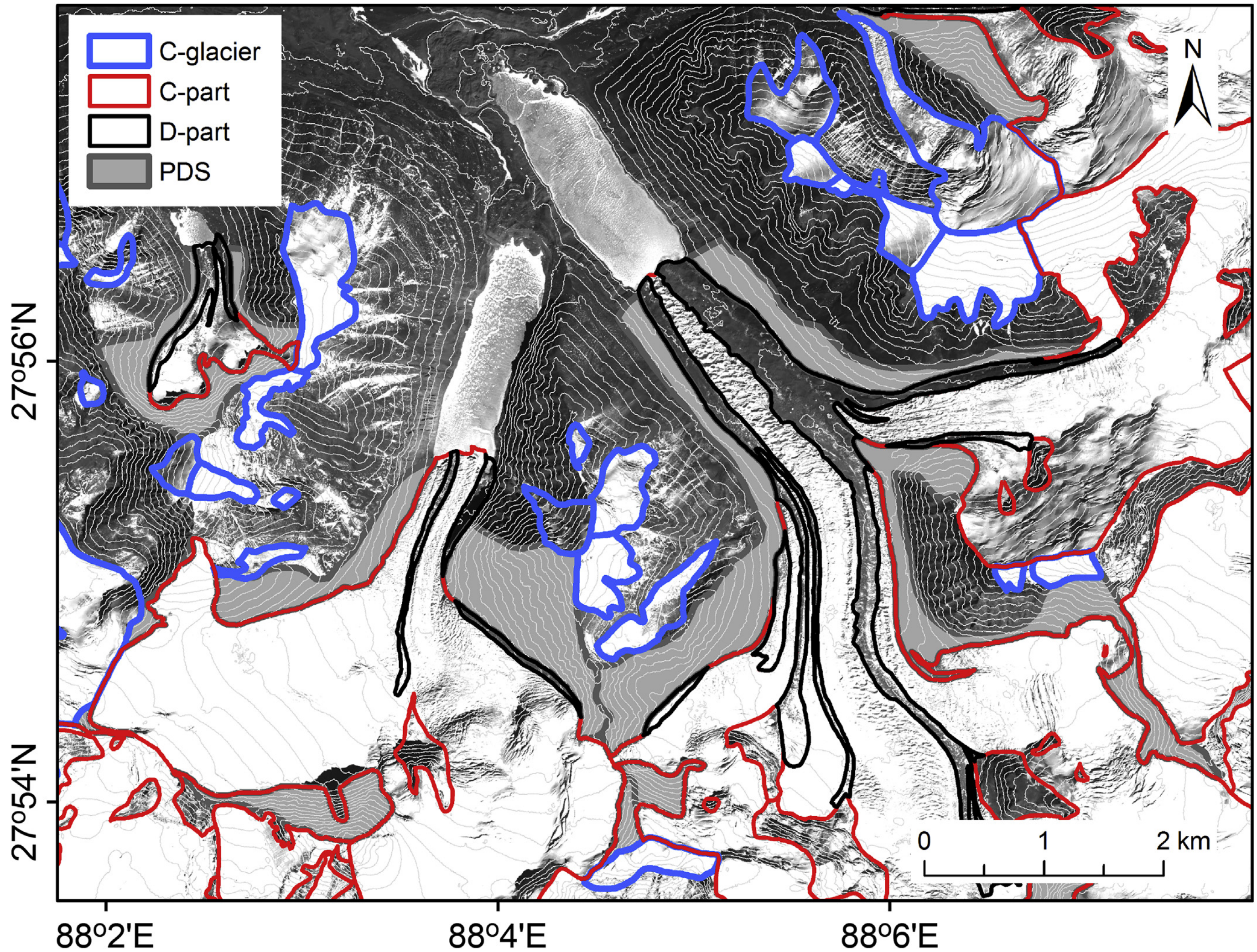

Fig. 2. Example of delineation. The background image is an ALOS-PRISM image taken on 31 October 2010. Blue lines delineate C-glaciers, whereas red and black lines delineate the C- and D-parts of D-glaciers, respectively. Gray polygons delineate PDS slope areas. (For interpretation of the references to colour in this figure legend, the reader is referred to the web version of this article.)

Table 1
Summary of the ALOS (AGI: this study), GAMDAM (GGI: Nuimura et al., 2015), and IGI (ICIMOD: Bajracharya et al., 2014a) glacier inventories in the Eastern Himalayas.

	AGI				GGI	IGI
	Total	C-glacier	D-glacier			
Number	5301	4459	842		4526	4690
Area (km^2)	5691 ± 893	1853 ± 141	3839 ± 753		5422	6212
			C-part	D-part		
			2867 ± 167	971 ± 237		

smaller debris-free glaciers, whereas the D-glaciers are symmetrically distributed over different glacier sizes (Fig. 3). The cumulative area of the D-glaciers is almost double that of the C-glaciers. The median areas of the glaciers (0.1 km^2 for C-glaciers and 1.5 km^2 for D-glaciers) are much smaller than their respective mean areas (0.4 km^2 for C-glaciers and 4.5 km^2 for D-glaciers), further highlighting the considerable extent smaller glaciers across our study area.

Although the AGI shows a higher number of glaciers (5301) than the GGI (4526) and IGI (4690), this is most likely the result of the finer-resolution (2.5 m) images used for the delineation. In addition, the total areal coverage (5691 ± 893 km^2) of the AGI glaciers was less than that of IGI (6212 km^2), but greater than that of GGI glaciers (5422 km^2: Table 1). These three inventories show similar hypsometric profiles, although a significant discrepancy was observed between the AGI and GGI at higher elevations, possibly because of the slope limitation associated with the upper glacier boundary in the GGI. The IGI overestimates the total areal coverage at all elevations (Fig. 4a).

Fig. 4a also shows the hypsometry of the C- and D-glaciers, with the D-glaciers exhibiting a broader elevation distribution than the C-glaciers, although both glacier groups have their maximum areal coverage at similar elevations (5400–5600 m a.s.l.). The median elevation of the glaciers in this region is 5605 ± 402 m a.s.l., with D-glaciers (5484 ± 369 m a.s.l.) clearly situated at lower elevations than C-glaciers (5627 ± 404 m a.s.l.: Table 2). The mean slope of the glaciers is 30° ± 9°, with the D-glaciers (26° ± 6°) possessing distinctly flatter profiles than the C-glaciers (31° ± 9°).

3.2. PDS slope and extent of debris cover

The 842 D-glaciers were further separated into their respective C- and D-parts, with the C-part covering 0.01–80.9 km^2 (mean area

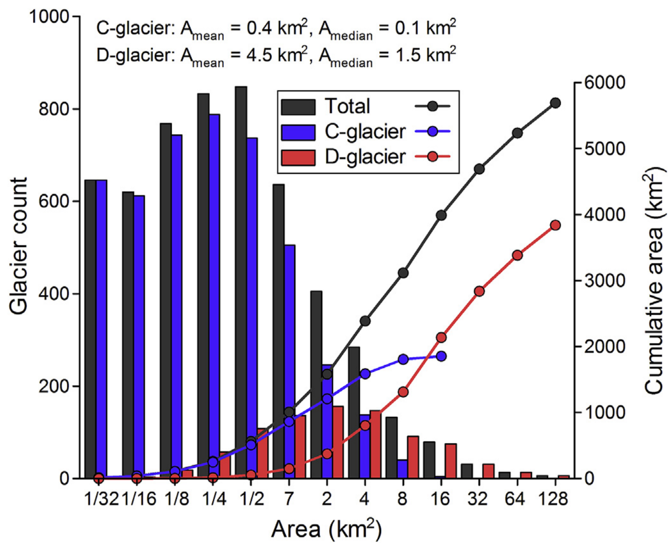

Fig. 3. Size distribution of the ALOS glacier inventory, showing the total (black bars), C-glacier (blue bars), and D-glacier (red bars) components on the left axis. Cumulative areas for the same three datasets (illustrated as circles and lines) are defined on the right axis. (For interpretation of the references to colour in this figure legend, the reader is referred to the web version of this article.)

The average gradient of the D-part (22° ± 8°) is much gentler than that of the C-part (30° ± 8°: Table 2). Although these gradients seem steeper than what is generally observed on valley glaciers, this is the result of the DEM-based calculation. The irregular topography of debris-covered glaciers (including ice cliffs and supraglacial ponds) results in a heterogeneous surface slope pattern that generally causes the DEM-based slope gradient to be steeper than the gradient along the flow line (Salerno et al., 2017). Previously published glacier inventories have similar values for the glacier slope gradient because the same DEM-based approach was used to calculate these gradients as attribute data so that these show similar values (AGI = 31°, RGI = 26°, ICI = 30°, GGI = 28° for C-glaciers).

The coupling of hillslopes and glacier dynamics influences the extent of Asian debris-covered glaciers, as Scherler et al. (2011b) found positive correlations between the debris-covered areas and hillslope angles of ice-free areas above the snowline, and also with the percentage of ice-free areas in the accumulation area. In this study, we first analyzed the relationships between glacier size, debris-covered area, and PDS slope area to determine how these correlate with each other in the Eastern Himalayas (Fig. 5). The relationship between debris-covered area and glacier size (Fig. 5a, n = 842) is similar to that reported by Scherler et al. (2011b), although they analyzed a broader region across high mountain Asia

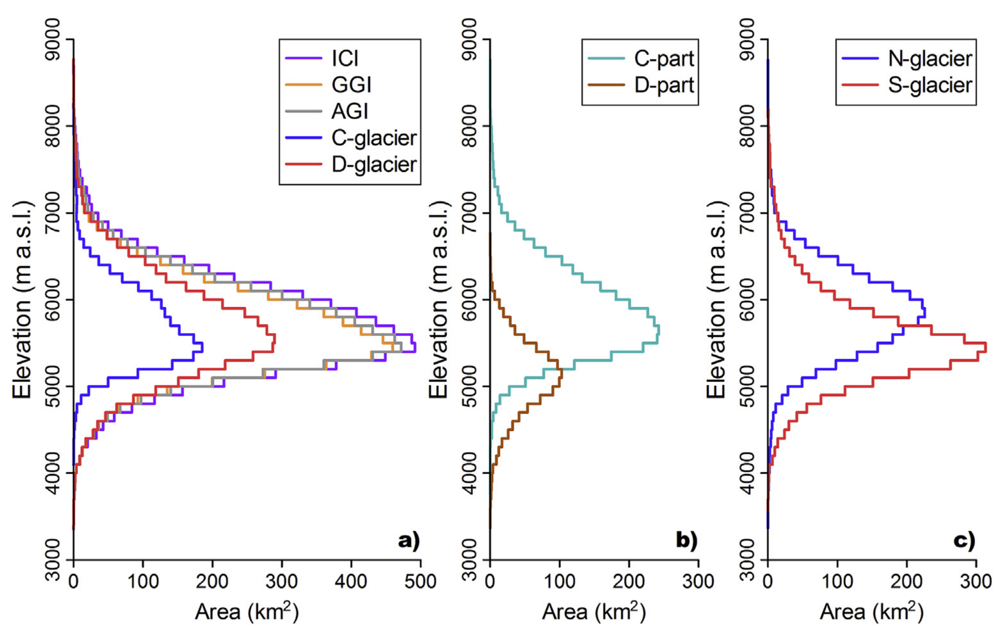

Fig. 4. Hypsometry of: (a) the ALOS glacier inventory (AGI: gray), with the profiles of C-glaciers (blue) and D-glaciers (red) included, compared with the ICIMOD (ICI: purple) and GAMDAM (GGI: orange) glacier inventories, (b) C-part (teal) and D-part (brown) of the D-glaciers, and (c) N-glaciers (blue) and S-glaciers (red). (For interpretation of the references to colour in this figure legend, the reader is referred to the web version of this article.)

of 3.4 km^2) of a given glacier, whereas the D-part covered only 0.01–27.2 km^2 (mean area 1.2 km^2), for total areas of 2867 ± 167 km^2 and 971 ± 236 km^2, respectively (Table 2). The C- and D-parts of the D-glaciers show distinct differences in their maximum areal coverage at the upper (5600–5700 m a.s.l.) and lower elevation (5100–5200 m a.s.l.) modes (Fig. 4b), resulting in median elevations of 5608 ± 336 m and 5198 ± 358 m a.s.l. (Table 2), respectively. Interestingly, we found that the hypsometry of the C-part is identical to that of C-glaciers below 5400 m a.s.l. (Fig. 4a and b), indicating that a snowline exists in this elevation range, with the D-part of D-glaciers forming at lower elevations.

(Fig. 3a of their study). Both the debris-covered area (Fig. 5a, r = 0.77, p < 0.001) and PDS slope area (Fig. 5b, r = 0.83, p < 0.001) are strongly correlated with the associated glacier size. If a topographic similarity is shared among Himalayan debris-covered glaciers, the obvious relationship is that larger glaciers have larger areas of both debris cover and PDS slope. Despite these strong correlations, however, it should be noted that the glacier area scales range over two orders of magnitude when comparing these two metrics; i.e., 100%–1% for debris-cover, and × 10 to × 0.1 for PDS (Fig. 5a and b). The relationship between the areas of debris cover and PDS slope shows that the majority falls within the range of one

Table 2
Regional statistics of the ALOS glacier inventory. The error represents the standard deviation for both the median elevation and gradient values. The value in parentheses depicts the number of glaciers in the corresponding massifs.

Regions	Langtang	Khumbu	Kan-Sikkim	Bhutan	Total
Glacier area (km^2)	901 ± 149 (704)	1847 ± 291 (1497)	1355 ± 208 (1358)	1587 ± 243 (1742)	5691 ± 893 (5301)
C-type	269 ± 20 (536)	495 ± 38 (1247)	475 ± 36 (1157)	615 ± 48 (1519)	1853 ± 141 (4459)
D-type	632 ± 129 (168)	1352 ± 254 (250)	880 ± 172 (201)	972 ± 196 (223)	3838 ± 752 (842)
C-part	448	990	675	752	2867 ± 167
D-part	184	362	204	220	971 ± 236
Median elevation (m a.s.l.)	5513 ± 391	5705 ± 444	5637 ± 392	5531 ± 349	5605 ± 402
C-type	5580 ± 375	5736 ± 453	5654 ± 402	5537 ± 344	5627 ± 404
D-type	5301 ± 369	5542 ± 363	5539 ± 305	5507 ± 385	5484 ± 369
C-part	5463 ± 341	5672 ± 350	5644 ± 280	5612 ± 332	5608 ± 336
D-part	4981 ± 326	5266 ± 345	5246 ± 323	5252 ± 356	5197 ± 358
Gradient (degree)	32 ± 8	31 ± 9	30 ± 8	26 ± 7	30 ± 9
C-type	32 ± 9	32 ± 9	31 ± 8	27 ± 7	31 ± 9
D-type	30 ± 7	28 ± 7	27 ± 5	23 ± 5	26 ± 6
C-part	33 ± 7	31 ± 8	30 ± 7	25 ± 6	30 ± 8
D-part	25 ± 9	22 ± 9	21 ± 8	19 ± 6	22 ± 8

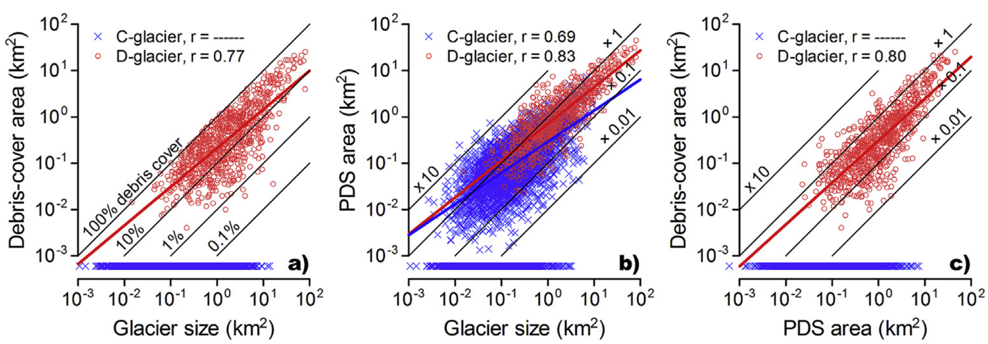

Fig. 5. Relationships between: a) debris-covered area and glacier size, b) PDS area and glacier size, and c) debris-covered area and PDS area of debris-covered glaciers (D-glaciers: circles) and debris-free glaciers (C-glaciers: crosses) across the Eastern Himalayas. Crosses forming a line at the bottom of each panel denote "zero area" for debris cover and PDS, which are conveniently depicted as minima on the log–log plots. Zero area data ($n = 1315$) are excluded from the regression line and correlation calculations for the C-glaciers in (b). The p-value is less than 0.001 in all cases.

order of magnitude ($\times$ 1 to $\times$ 0.1: Fig. 5c), suggesting that the debris cover and PDS slope have a more direct connection when compared with their respective relationships with glacier size. If we incorporate C-glaciers, which by definition have no debris-covered area, it is clear that glacier size is not a crucial factor for determining the debris-covered area (Fig. 5a). However, the PDS slope area was identified for 3144 C-glaciers (71% of total), whose distribution ranges over three orders of magnitude ($\times$ 10 to $\times$ 0.01), resulting in a reduced correlation coefficient than that observed for D-glaciers (Fig. 5b, $r = 0.69$, $p < 0.001$). The absence of a debris-covered area in the C-glaciers is most likely to be due to their smaller size and the gentler gradient of the PDS slope. The mean areas of the PDS slope and glacier size for C-glaciers are 0.17 km^2 and 0.42 km^2, respectively (including 1315 C-glaciers with no PDS slope), whereas those of the D-glaciers are 2.6 km^2 and 4.6 km^2, respectively, suggesting that both the source region for debris supply and the glacier surface where this debris can collect, may be insufficient. Furthermore, the gradient of the PDS slope for C-glaciers ($30° \pm 9°$) is statistically gentler than that for the D-glaciers ($37° \pm 7°$, $p < 0.001$), suggesting that the debris generated on the PDS slope may not fall onto the C-glacier surface (Fig. 6). We emphasize that our analysis quantifies the relationship between the areas of debris cover and PDS slope, whereas Scherler et al. (2011b) revealed the qualitative relationship through the debris-covered ratio and hillslope angle situated above the snowline. Scherler et al. (2011b) also analyzed less than 70 glaciers within the domain of this study (counted from Fig. 2a of their study), whereas we have analyzed more than 800 D-glaciers.

Although Scherler et al. (2011b) analyzed the ice-free slope situated above the snowline altitude, the PDS slope used in this study has no defined elevation constraint (Nagai et al., 2013). Therefore, it may be argued that the debris generated from a lateral moraine will not be a likely contributor to covering the glacier surface because the debris will not travel far enough to spread out

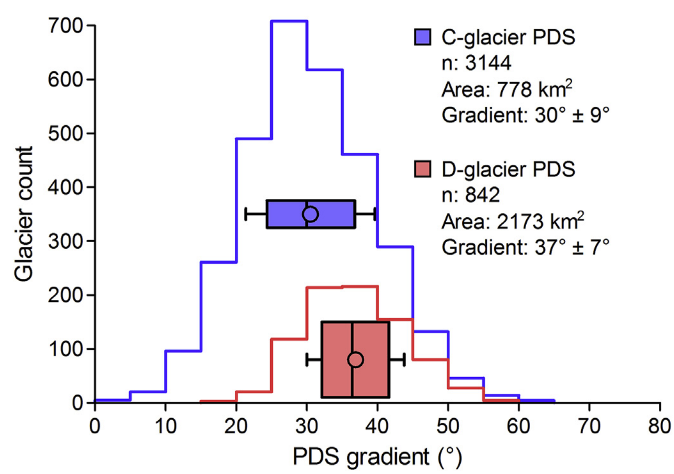

Fig. 6. Histogram and box plot of PDS slope gradients for C- and D-glaciers in the Eastern Himalayas. The box, thick line, circle, and whiskers denote the interquartile, median, mean, and standard deviations, respectively. The vertical width of the box denotes the total area of corresponding PDS slope.

Table 3
Regional statistics of northern-side and southern-side glaciers across the Himalayan barrier and their attributes (2006–2011). The error represents the standard deviation for both the median elevation and gradient. The value in parenthesis depicts the number of glaciers in the corresponding massifs.

Regions	Langtang	Khumbu	Kan-Sikkim	Bhutan	Total
Glacier area (km^2)					
Northern-side	335 ± 52 (218)	954 ± 142 (666)	416 ± 56 (486)	929 ± 46 (850)	2636 ± 397 (2220)
Southern-side	565 ± 95 (486)	892 ± 149 (831)	938 ± 152 (872)	657 ± 97 (892)	3054 ± 495 (3081)
Median elevation (m a.s.l.)					
Northern-side	5672 ± 419	5891 ± 474	5837 ± 346	5744 ± 334	5802 ± 399
Southern-side	5441 ± 356	5555 ± 355	5528 ± 370	5330 ± 222	5464 ± 341
Gradient (degree)					
Northern-side	30 ± 8	30 ± 8	31 ± 8	28 ± 7	30 ± 8
Southern-side	33 ± 9	32 ± 9	30 ± 8	25 ± 6	30 ± 8

Table 4
Correlation coefficient (r) between PDS slope area and D-part area for different aspects. The p-value is less than 0.001 in all cases.

Regions	LT	KB	KS	BT
All PDS slope	0.87	0.82	0.82	0.82
South-facing slope	0.68	0.65	0.64	0.87
North-facing slope	0.77	0.70	0.76	0.67

onto the central part of an irregular glacier surface. However, as illustrated in Fig. 2, debris that has fallen from a lateral moraine accumulates at the edges of the glacier, and is then conveyed and spread down-glacier along the glacier flow. This feature, termed elongated debris cover, is found on glaciers across the northern slope of the Himalayas (Nagai et al., 2013). These debris falls could occur frequently from lateral moraines because the inside slope tends to be steep and fresh enough to generate a gravity instability (Fujita et al., 2008). Heavy rains could also cause debris flows or falls from the loose slope of a lateral moraine, although these would be rare. The amount of debris would be significantly less than that from the upper ice-free slope, thus causing the debris cover originating from a lateral moraine to be masked by debris originating from the upper slope, particularly across the southern slope of the Himalayas (Nagai et al., 2013). Although the contribution of debris originating from a lateral moraine to the entire debris-covered area of the Himalayan glaciers would be small, the PDS slope neighboring the ablation zone contributes to the formation of debris-covered area, and thus should not be ignored.

3.3. Glaciers on northern and southern slopes

To understand the effect of large-scale topography on the extent of debris cover in the Eastern Himalayas, we divided the study area into two zones, with the main Eastern Himalayan range acting as a climatic barrier. We identified 2220 N-glaciers, covering an area of 2637 ± 398 km^2, and 3081 S-glaciers, covering an area of 3055 ± 495 km^2 (Table 3). Fig. 4c shows that the maximum coverage of the S-glaciers occurs at lower elevations (5400–5500 m a.s.l.) than that of the N-glaciers (5800–5900 m a.s.l.), with median elevations of 5465 ± 341 m and 5802 ± 399 m a.s.l., respectively (Table 3). These differences in median elevations are caused partly by differences in the mean local relief, which is higher on the southern slope than it is on the northern slope (Scherler et al., 2011b), and partly by the sharp decline in precipitation along the northern slope of the Himalayan barrier (Maussion et al., 2013).

3.4. Regional trends

3.4.1. C- and D-glaciers

The far-western LT massif has fewer clusters of glaciers, in terms of both area and number, compared with the other three massifs

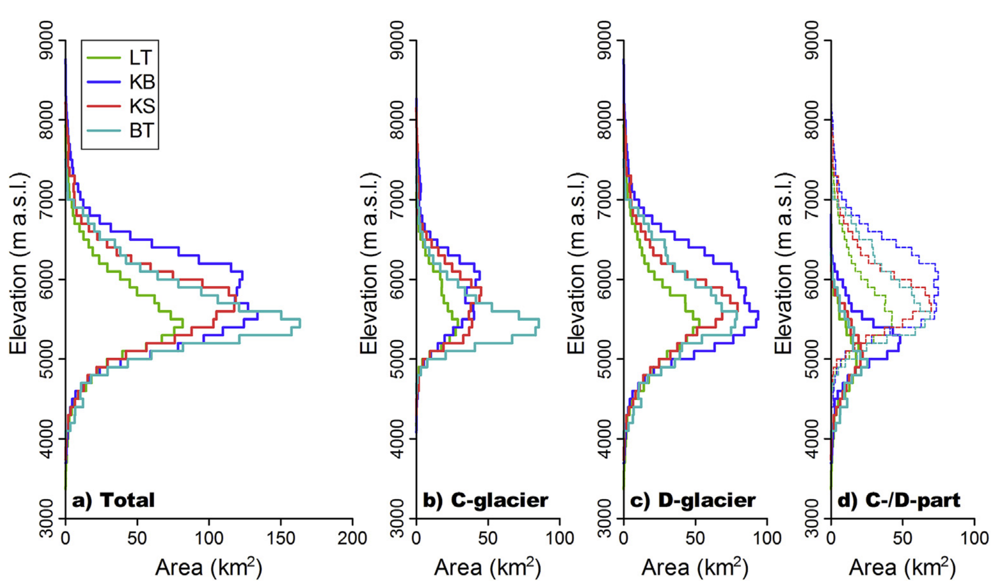

Fig. 7. Hypsometry of: (a) all glaciers across the study region, (b) C-glaciers, (c) D-glaciers, and (d) the C-part (thin dashed lines) and D-part (thick solid lines) of the D-glaciers for the four massifs (LT: Langtang, KB: Khumbu, KS: Kanchenjunga-Sikkim, and BT: Bhutan).

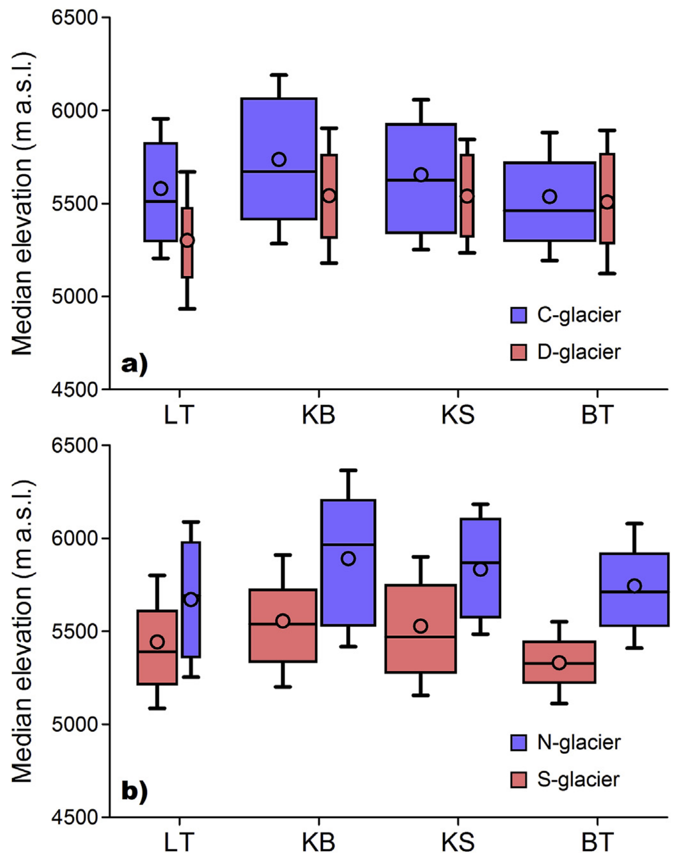

Fig. 8. Box plots of median elevation for: (a) C-glaciers (blue) and D-glaciers (red) and (b) S-glaciers (red) and N-glaciers (blue) across the four massifs (LT: Langtang, KB: Khumbu, KS: Kanchenjunga-Sikkim, and BT: Bhutan). The box, thick line, circle, and whiskers denote the interquartile, median, mean, and standard deviations, respectively. The width of the box denotes the number of corresponding glaciers. (For interpretation of the references to colour in this figure legend, the reader is referred to the web version of this article.)

(Table 2). The massifs are dominated mainly by the D-glaciers (67% in total), with the greatest coverage observed across the KB massif (73%) followed by the LT (70%), KS (65%), and BT (61%) massifs. The D-part coverage also shows a gentle decline from west to east (LT = 29%, KB = 27%, KS = 23%, and BT = 23%).

3.4.2. Hypsometry

Fig. 7a shows the hypsometry of the four massifs, with most of the glaciers situated between 5000 and 6500 m a.s.l. The largest glaciers in the BT and LT massifs are situated at lower elevations (5400–5500 m a.s.l.) than those in the KB and KS massifs (5700–5800 m a.s.l.). The hypsometry of the C-glaciers shows that the larger glaciers occur at lower elevations (5400–5500 m a.s.l.) in the BT massif (Fig. 7b), whereas the symmetrical, but highly variable, coverage of the D-glaciers is found across all massifs (Fig. 7c). Similar elevation profiles are found below 5000 m a.s.l. across all massifs, whereas the elevation profile is highly variable for both C- and D-glaciers above 5000 m a.s.l. Fig. 7d depicts the hypsometry of both the C- and D-parts of the D-glaciers, where the D-part is evident at lower elevations than the C-part. Although the D-part has identical altitudinal profiles (except KB), the C-part has highly variable altitudinal coverage due to the presence of high mountain peaks across the region.

3.4.3. Median elevations

The median elevations of the D-glaciers are clearly lower than those of the C-glaciers, especially across the western massifs (LT and KB), whereas similar median elevations are observed across the eastern massifs (KS and BT: Fig. 8a). The statistical analysis, based on a 0.25° weighed area, shows that the median elevation of the C-glaciers follows a decreasing trend ($r = -0.25$, $p < 0.1$) towards the east, whereas there is no significant trend for the D-glaciers, implying that the median elevation of the D-glaciers is stable across the study area. However, the median elevation of the S-glaciers is distinctly lower than that of the N-glaciers across the Himalayan barrier (Fig. 8b). From west to east, we find a significant decreasing trend ($r = -0.48$, $p < 0.01$) in median elevation on the southern side

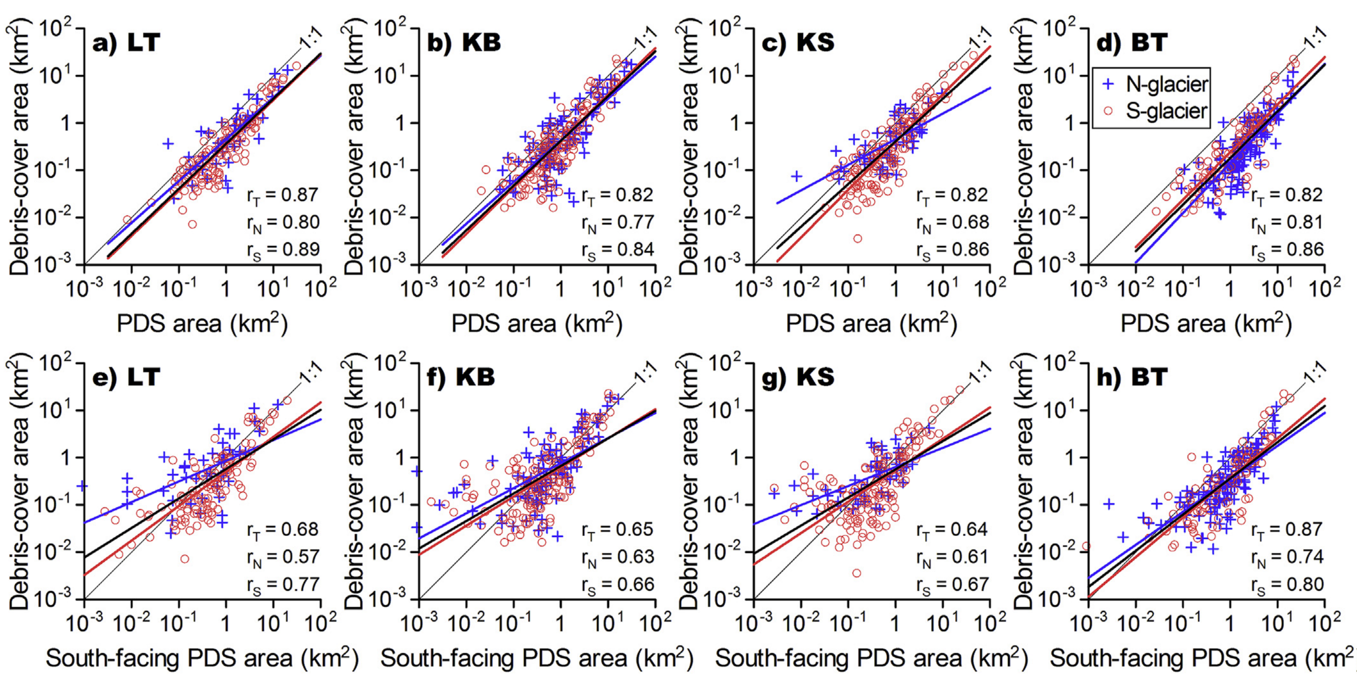

Fig. 9. Scatter plots between debris-cover area and PDS area for (a–d) all aspects and (e–h) south-facing aspects (90–270°, clockwise) across the four massifs (LT: Langtang, KB: Khumbu, KS: Kanchenjunga-Sikkim, and BT: Bhutan). The red, blue, and black lines denote regression lines for the N-glacier (red crosses), S-glacier (blue open circle) and both glaciers, respectively. Correlation coefficients are calculated between the debris-cover area and corresponding PDS area for the total glaciers (r_T), N-glacier (r_N) and S-glacier (r_S), respectively. The p-value is less than 0.001 in all cases. (For interpretation of the references to colour in this figure legend, the reader is referred to the web version of this article.)

of the mountain barrier, whereas no significant trend is found on the northern side. This indicates the stable nature of glaciers on the northern side of the mountain barrier.

3.5. Relationship between PDS slope and debris-covered area

We checked the normality of both the PDS slope area and D-part area using a simple quantile–quantile plot (not shown), and found that they are skewed and widely distributed, and similar to the area distribution patterns illustrated in Fig. 3. The data were therefore normalized using the log-transformation method (Venables and Ripley, 2002; Salerno et al., 2016). Significant positive correlations were found between the PDS slope areas and D-part areas by establishing a relationship using Pearson correlation coefficient (r). Our analysis implies that larger PDS slopes tend to supply greater amounts of debris mantle to the glacier surface, thus forming a greater extent of the D-part (Fig. 9a–d). This relationship is strong for all massifs (LT: $r = 0.87$, $p < 0.001$; KB: $r = 0.82$, $p < 0.001$; KS: $r = 0.82$, $p < 0.001$; and BT: $r = 0.82$, $p < 0.001$). The slightly stronger correlations for the western massifs may be due to the larger PDS areas and steeper PDS gradients (Fig. 10a), which probably provide sufficient debris mantle to the glaciers (Fig. 10b). In a similar study, Scherler et al. (2011b) found positive correlations between debris-covered areas and the hillslope gradient of ice-free areas above the snowline and with the percentage of ice-free areas in the accumulation area. We also tested the relationship between the percentage of debris coverage and the mean gradient of the PDS slope. However, we found no good correlation (LT: $r = 0.05$; KB: $r = 0.18$; and KS: $r = 0.27$, $p < 0.001$), except for a slightly better correlation for the Bhutan massif (BT: $r = 0.43$, $p < 0.001$).

We further analyzed the glaciers on the two slopes divided by the large mountain barrier, the N- and S-glaciers, and investigated their respective relationships between the D-part area and PDS area. Although both glaciers show strong positive correlations between the D-part area and PDS slope area, the S-glaciers tend to show higher correlations than the N-glaciers for all massifs (Fig. 10c), which is probably due to a lower D-part area in the N-glaciers than in the S-glaciers, with the exception of the KB massif (Fig. 9a–d). This result suggests that the S-glaciers receive more debris than the N-glaciers, and is in agreement with what Nagai et al. (2013) demonstrated in the Bhutan Himalaya. We therefore analyzed the relationship between the south-facing PDS area (90–270°, clockwise) and the D-part area (Fig. 9e–h). The correlation is slightly improved ($r = 0.87$, $p < 0.001$) over that for the total PDS slope area ($r = 0.82$, $p < 0.001$) for the far-eastern BT massif, whereas noticeably lower values are found for the other massifs (LT: $r = 0.68$, $p < 0.001$; KB: $r = 0.65$, $p < 0.001$; and KS: $r = 0.64$, $p < 0.001$: Table 4). According to Nagai et al. (2013), the south-facing PDS slope areas are distributed at limited locations and primarily serve as a source for stripe-like supraglacial debris in the N-glaciers. Similarly, rockfalls from the PDS in the ablation area do not travel far, and thus will not contribute to the formation of debris cover in the central part, but rather the formation of stripe-like or side-located supraglacial debris in a limited way. We believe that the stripe-like debris cover in the N-glaciers in the Himalayas results from the limited contributions of the PDS slopes. However, the south-facing PDS in the S-glaciers form the headwall, with rockfalls onto the accumulation area that may become entrained into the glacier ice. Those rocks reappear at the surface in the ablation area, thus yielding extensive debris cover (Nagai et al., 2013). Diurnal freeze–thaw cycles could be one plausible explanation for the effect of south-facing PDS slopes on debris cover (Nagai et al., 2013). There are also other potential periglacial processes that could produce debris mantle. For instance, frost cracking by ice segregation in the near-surface area is the major cause of rock fracture in cold humid regions (Murton et al., 2006; Hales and Roering, 2007), and subglacial plowing and scouring is a possible source of debris mantle, although it is difficult to quantify these contributions.

3.6. Effect of aspect and gradient of PDS slope on formation of debris-covered areas

To understand the effects of the aspect and gradient of the PDS slope on formation of debris cover, following the analysis of Nagai et al. (2013), we calculated the correlation coefficients between the D-part area and its corresponding aspect and gradient for both S- and N-glaciers along the Himalayan barrier. Fig. 11a and b shows the correlation coefficients between the PDS slope area and

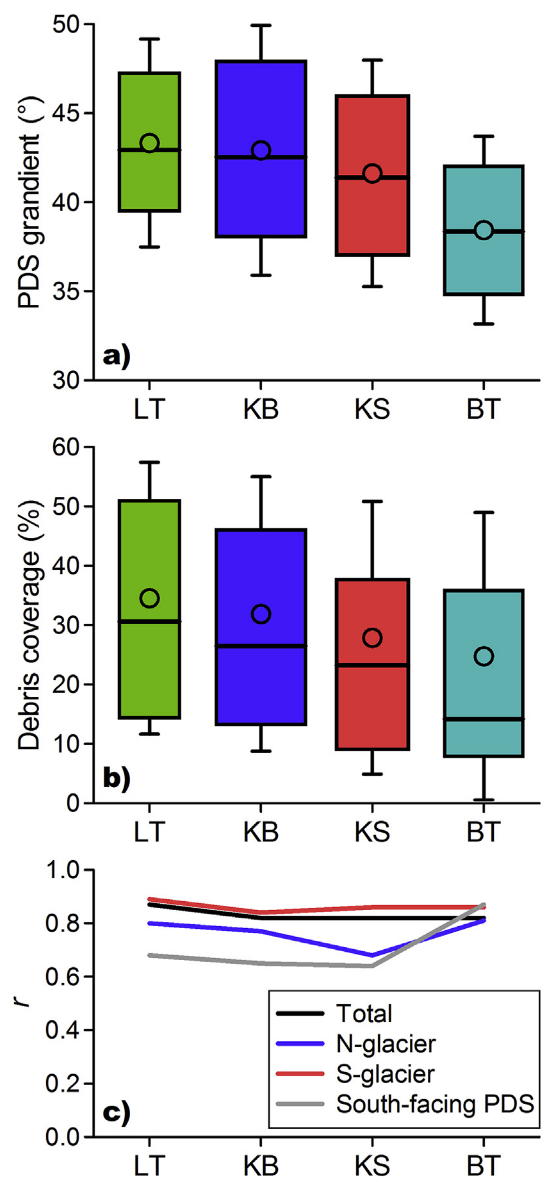

Fig. 10. Box plots of (a) PDS gradient and (b) debris coverage (%), and (c) correlation coefficient (r) between debris-covered area and corresponding PDS area for the total, S-glaciers, and N-glaciers across the four massifs (LT: Langtang, KB: Khumbu, KS: Kanchenjunga-Sikkim, and BT: Bhutan). The gray line in (c) denotes the correlation coefficient for the south-facing PDS area and debris-covered area. The box, thick line, circle, and whiskers denote the interquartile, median, mean, and standard deviations, respectively. The width of the box denotes the number of corresponding glaciers.

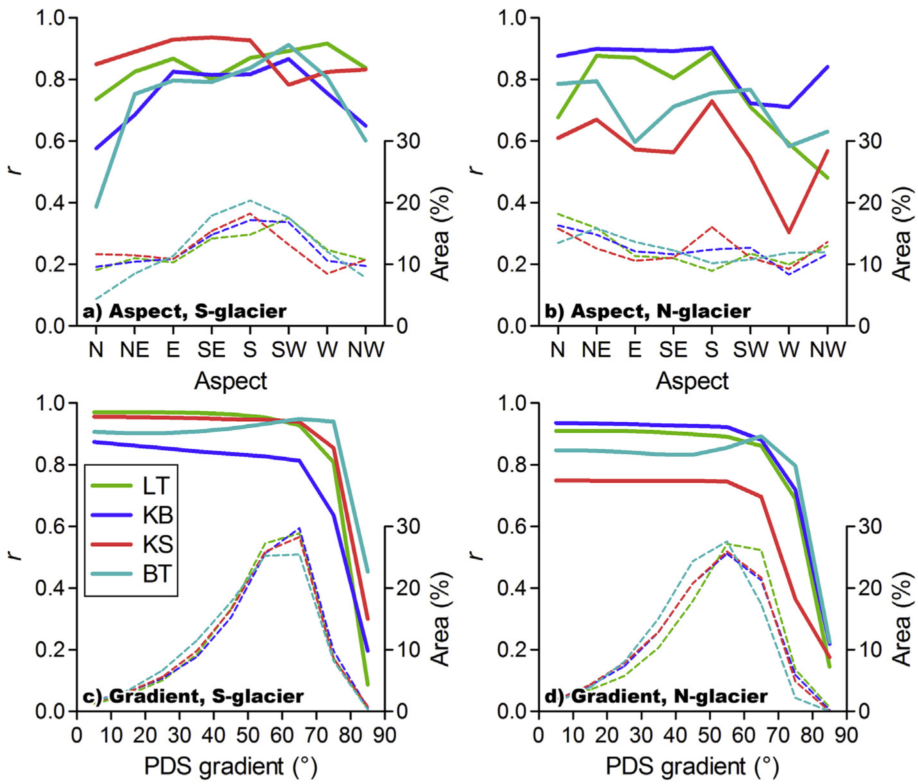

Fig. 11. Correlation coefficient (*r* on left axes, thick lines on plots) between debris-covered area and corresponding PDS slope area at different aspects (a and b, upper panels), and for different gradient ranges (c and d, lower panels) for both the S-glaciers (a and c, left panels) and N-glaciers (b and d, right panels) across the four massifs (LT: Langtang, KB: Khumbu, KS: Kanchenjunga-Sikkim, and BT: Bhutan). PDS slope area coverage is also shown (% on right axes, thin dashed lines).

corresponding D-part area for S- and N-glaciers, at different aspects. The correlation values are consistently higher for S-glaciers than they are for N-glaciers, and this is caused by the larger PDS area on the southern side of the Himalayan barrier. Across the far-eastern BT massif, SW-facing PDS slopes have a high correlation with the D-part area, which was the main finding of Nagai et al. (2013), whereas KS, KB, and LT have higher correlation values with SE-, SW-, and W-facing PDS slopes, respectively. Nagai et al. (2013) proposed that SW-facing PDS slopes controlled the D-part area in the Bhutan Himalaya, but this cannot be directly applied to the other Himalayan regions. For both the S- and N-glaciers, a higher correlation value is accompanied by a larger PDS area. Overall, larger PDS areas (%) with slopes oriented SE to W tend to supply more debris to the glaciers. Similarly, a good association between a decreasing correlation coefficient and decreasing PDS area (%) is also found for the N-glaciers (Fig. 11b).

Fig. 11c and d depict the correlation coefficients between PDS slope area and D-part area for both S- and N-glaciers in different gradient categories. The PDS areas with gradients less than 65° and 55° are the main sources of formation of debris cover in the S- and N-glaciers, respectively. The correlation coefficient decreases as these gradients increase because of the decrease in PDS area coverage (%). The lower correlation value for the N-glaciers may be caused by the presence of more snow coverage in its accumulation zone, as a flatter slope is expected with greater snow coverage, and thus tends to produce less debris mantle. Conversely, steep slopes with less snow coverage in S-glaciers may facilitate more frequent rock falls and avalanches. Although 30% of the PDS area lies at 60–70° in the S-glaciers and 50–60° in the N-glaciers, there were no evident correlations for those particular gradient ranges. Correlation values are similar for LT and BT, but notably different for KB and KS in the S- and N-glaciers. Across KB, correlation values are higher for N-glaciers, whereas they are higher for S-glaciers across KS.

4. Conclusions

For this study, we used 104 high-resolution (2.5 m) ALOS-PRISM images to manually digitized 5301 glaciers (5691 ± 893 km^2) on both sides of the mountain barrier in the middle of the Eastern Himalayan range, and covering the political territories of Bhutan, India, China, and Nepal. We identified 4459 clean-type and 842 debris-covered glaciers, covering 1853 ± 141 km^2 and 3839 ± 753 km^2, respectively, across the four massifs in our study region. The novel finding of this study is that an area of 971 ± 237 km^2 is covered by a debris mantle. The regional elevation profile shows that the glaciers on the southern slope of the mountain barrier are generally situated at lower elevations when compared with those on the northern slope.

The debris-covered glaciers were further divided into their respective debris-covered and debris-free parts to examine formation of debris cover on a regional scale. The potential debris supply (PDS) slope, which is the probable cause of formation of debris cover proposed for the Bhutan Himalaya (Nagai et al., 2013), was used and extended to our study region. We found significant positive correlations between PDS slope area and the debris-covered area of glaciers, suggesting that a larger PDS area tends to produce more debris mantle and supplies it to the glaciers. This relationship is stronger across the western massifs than it is across the eastern ones, and this may be the result of the larger PDS areas and steeper slopes to the west. Further analysis showed that south-facing PDS slope are more closely correlated to their corresponding debris-covered glacier areas. Therefore, we have provided further evidence that the debris-covered area of glaciers is strongly controlled by south-to west-facing PDS slopes across the different massifs. Consequently, we believe that it will be necessary to extend this study to the Western Himalayas and Karakorum, where numerous debris-covered glaciers exist under different climates, if we are to better understand the contribution of PDS slopes to debris-covered glacier formation.

Acknowledgements

We are grateful to F. Salerno and two anonymous reviewers for their thoughtful comments. This study was supported by a grant from the Next Generation World-Leading Researchers Funding Program (NEXT Program, GR052) and JSPS-KAKENHI grant Number 26257202.

References

Bajracharya, S.R., Maharjan, S.B., Shrestha, F., Bajracharya, O.R., Baidhya, S., 2014a. Glacier Status in Nepal and Decadal Change from 1980 to 2010 Based on Landsat Data. International Centre for Integrated Mountain Development (ICIMOD), Kathmandu, p. 100.

Bajracharya, S.R., Maharjan, S.B., Shrestha, F., 2014b. The status and decadal change of glaciers in Bhutan from the 1980s to 2010 based on satellite data. Ann. Glaciol. 55 (66), 159–166. http://dx.doi.org/10.3189/2014AoG66A125.

Bolch, T., Kulkarni, A., Kaab, A., Huggel, C., Paul, F., Cogley, J.G., Frey, H., Kargel, J.S., Fujita, K., Scheel, M., Bajracharya, S., Stoffel, M., 2012. The state and fate of Himalayan glaciers. Science 336, 310–314. http://dx.doi.org/10.1126/science.1215828.

Cogley, J.G., 2016. Glacier shrinkage across high mountain Asia. Ann. Glaciol. 57 (71), 41–49. http://dx.doi.org/10.3189/2016AoG71A040.

Fujita, K., 2008. Effect of precipitation seasonality on climatic sensitivity of glacier mass balance. Earth Planet. Sci. Lett. 276, 14–19. http://dx.doi.org/10.1016/j.epsl.2008.08.028.

Fujita, K., Suzuki, R., Nuimura, T., Sakai, A., 2008. Performance of ASTER and SRTM DEMs, and their potential for assessing glacial lakes in the Lunana region, Bhutan Himalaya. J. Glaciol. 54, 220–228. http://dx.doi.org/10.3189/002214308784886162.

Fujita, K., Sakai, A., Nuimura, T., Yamaguchi, S., Sharma, R.R., 2009. Recent changes in Imja Glacial Lake and its damming moraine in the Nepal Himalaya revealed by in situ surveys and multi-temporal ASTER imagery. Environ. Res. Lett. 4, 045205. http://dx.doi.org/10.1088/1748-9326/4/4/045205.

Fujita, K., Nuimura, T., 2011. Spatially heterogeneous wastage of Himalayan glaciers. Proc. Natl. Acad. Sci. U. S. A. 108 (34), 14011–14014. http://dx.doi.org/10.1073/pnas.1106242108.

Fujita, K., Sakai, A., 2014. Modelling runoff from a Himalayan debris-covered glacier. Hydrol. Earth Syst. Sci. 18, 2679–2694. http://dx.doi.org/10.5194/hess-18-2679-2014.

Gardelle, J., Berthier, E., Arnaud, Y., Kääb, A., 2013. Region-wide glacier mass balances over the Pamir-Karakoram-Himalaya during 1999-2011. Cryosphere 7, 1263–1286. http://dx.doi.org/10.5194/tc-7-1263-2013.

Guo, W., Liu, S., Xu, J., Wu, L., Shangguan, D., Yao, X., Wei, J., Bao, W., Yu, P., Liu, Q., Jiang, Z., 2015. The second Chinese glacier inventory: data, methods and results. J. Glaciol. 61, 357–371. http://dx.doi.org/10.3189/2015JoG14J209.

Hales, T.C., Roering, J.J., 2007. Climatic controls on frost cracking and implications for the evolution of bedrock landscapes. J. Geophys. Res. 112, F02033. http://dx.doi.org/10.1029/2006JF000616.

Immerzeel, W.W., Pellicciotti, F., Bierkens, M.F.P., 2013. Rising river flows throughout the twenty-first century in two Himalayan glacierized watersheds. Nat. Geosci. 6, 742–745. http://dx.doi.org/10.1038/ngeo1896.

Kääb, A., Berthier, E., Nuth, C., Gardelle, J., Arnaud, Y., 2012. Contrasting patterns of early twenty-first-century glacier mass change in the Himalayas. Nature 488, 495–498. http://dx.doi.org/10.1038/nature11324.

Luedeling, E., Siebert, S., Buerkert, A., 2007. Filling the voids in the SRTM elevation model – a TIN-based delta surface approach. ISPRS J. Photogrammetry Remote Sens. 62, 283–294. http://dx.doi.org/10.1016/j.isprs.jprs.2007.05.004.

Mattson, L.E., Gardner, J.S., Young, G.J., 1993. Ablation on Debris Covered Glaciers: an Example from the Rakhiot Glacier, Punjab, Himalaya, vol. 218. IAHS Publication, pp. 289–296.

Maussion, F., Scherer, D., Mölg, T., Collier, E., Curio, J., Finkelnburg, R., 2013. Precipitation seasonality and variability over the Tibetan Plateau as resolved by the high Asia reanalysis. J. Clim. 27, 1910–1927. http://dx.doi.org/10.1175/JCLI-D-13-00282.1.

Murton, J.B., Peterson, R., Ozouf, J.C., 2006. Bedrock fracture by ice segregation in cold regions. Science 314, 1127–1129. http://dx.doi.org/10.1126/science.1132127.

Nagai, H., Fujita, K., Nuimura, T., Sakai, A., 2013. Southwest-facing slopes control the formation of debris-covered glaciers in the Bhutan Himalaya. Cryosphere 7, 1303–1314. http://dx.doi.org/10.5194/tc-7-1303-2013.

Nagai, H., Fujita, K., Sakai, A., Nuimura, T., Tadono, T., 2016. Comparison of multiple glacier inventories with a new inventory derived from high-resolution ALOS imagery in the Bhutan Himalaya. Cryosphere 10, 65–85. http://dx.doi.org/10.5194/tc-10-65-2016.

Nuimura, T., Fujita, K., Yamaguchi, S., Sharma, R.R., 2012. Elevation changes of glaciers revealed by multitemporal digital elevation models calibrated by GPS survey in the Khumbu region, Nepal Himalaya, 1992–2008. J. Glaciol. 58, 648–656. http://dx.doi.org/10.3189/2012JoG11J061.

Nuimura, T., Sakai, A., Taniguchi, K., Nagai, H., Lamsal, D., Tsutaki, S., Kozawa, A., Hoshina, Y., Takenaka, S., Omiya, S., Tsunematsu, K., Tshering, P., Fujita, K., 2015. The GAMDAM glacier inventory: a quality-controlled inventory of Asian glaciers. Cryosphere 9, 849–864. http://dx.doi.org/10.5194/tc-9-849-2015.

Nuimura, T., Fujita, K., Sakai, A., 2017. Downwasting of the debris-covered area of Lirung glacier In Langtang Valley, Nepal Himalaya, from 1974 to 2010. Quat. Int. 455, 93–101. http://dx.doi.org/10.1016/j.quaint.2017.06.066.

Ojha, S., Fujita, K., Asahi, K., Sakai, A., Lamsal, D., Nuimura, T., Nagai, H., 2016. Glacier area shrinkage in eastern Nepal Himalaya since 1992 using high-resolution inventories from aerial photographs and ALOS satellite images. J. Glaciol. 62, 512–524. http://dx.doi.org/10.1017/jog.2016.61.

Paul, F., Barrand, N.E., Baumann, S., Berthier, E., Bolch, T., Casey, K., Frey, H., Joshi, S.P., Konovalov, V., Bris, R.L., Mölg, N., Nosenko, G., Nuth, C., Pope, A., Racoviteanu, A., Rastner, P., Raup, B., Scharrer, K., Steffen, S., Winsvold, S., 2013. On the accuracy of glacier outlines derived from remote-sensing data. Ann. Glaciol. 54 (63), 171–182. http://dx.doi.org/10.3189/2013AoG63A296.

Pfeffer, W.T., Arendt, A.A., Bliss, A., Bolch, T., Cogley, J.G., Gardner, A.S., Hagen, J., Hock, R., Kaser, G., Kienholz, C., Miles, E.S., Moholdt, G., Mölg, N., Paul, F., Radic, V., Rastner, P., Raup, B.H., Justin, R., Sharp, M.J., The Randolph Consortium, 2014. The Randolph Glacier Inventory: a globally complete inventory of glaciers. J. Glaciol. 60, 537–552. http://dx.doi.org/10.3189/2014JoG13J176.

Racoviteanu, A.E., Paul, F., Raup, B., Khalsa, S.J.S., Armstrong, R., 2009. Challenges and recommendations in mapping of glacier parameters from space: results of the 2008 Global Land Ice Measurements from Space (GLIMS) workshop, Boulder, Colorado, USA. Ann. Glaciol. 50 (53), 53–69. http://dx.doi.org/10.3189/172756410790595804.

Ragettli, S., Bolch, T., Pellicciotti, F., 2016. Heterogeneous glacier thinning patterns over the last 40 years in Langtang Himal. Cryosphere 10, 2075–2097. http://dx.doi.org/10.5194/tc-10-2075-2016.

Raup, B., Khalsa, S.J.S., 2010. GLIMS Analysis Tutorial. University of Colorado, National Snow and Ice Data Center, Boulder, Colorado.

Reuter, H.I., Nelson, A., Jarvis, A., 2007. An elevation of void-filling interpolation methods for SRTM data. Int. J. Geogr. Inf. Sci. 9, 983–1008. http://dx.doi.org/10.1080/13658810601169899.

Sakai, A., Nuimura, T., Fujita, K., Takenaka, S., Nagai, H., Lamsal, D., 2015. Climate regime of Asian glaciers revealed by GAMDAM glacier inventory. Cryosphere 9, 865–880. http://dx.doi.org/10.5194/tc-9-865-2015.

Salerno, F., Thakuri, S., Guyennon, N., Viviano, G., Tartari, G., 2016. Glacier melting and precipitation trends detected by surface area changes in Himalayan ponds. Cryosphere 10, 1433–1448. http://dx.doi.org/10.5194/tc-10-1433-2016.

Salerno, F., Thakuri, S., Tartari, G., Nuimura, T., Sunako, S., Sakai, A., Fujita, K., 2017. Debris-covered glacier anomaly? Morphological factors controlling changes in the mass balance, surface area, terminus position, and snow line altitude of Himalayan glaciers. Earth Planet. Sci. Lett. 471, 19–31. http://dx.doi.org/10.1016/j.epsl.2017.04.039.

Scherler, D., Bookhagen, B., Strecker, M.R., 2011a. Spatially variable response of Himalayan glaciers to climate change affected by debris cover. Nat. Geosci. 4, 156–159. http://dx.doi.org/10.1038/ngeo1068.

Scherler, D., Bookhagen, B., Strecker, M.R., 2011b. Hillslope-glacier coupling: the interplay of topography and glacial dynamics in high Asia. J. Geophys. Res. 116, F02019. http://dx.doi.org/10.1029/2010JF001751.

Shea, J.M., Immerzeel, W.W., Wagnon, P., Vincent, C., Bajracharya, S., 2015. Modelling glacier change in the Everest region, Nepal Himalaya. Cryosphere 9, 1105–1128. http://dx.doi.org/10.5194/tc-9-1105-2015.

Tachikawa, T., Kaku, M., Iwasaki, A., Gesch, D., Oimoen, M., Zhang, Z., Danielson, J., Krieger, T., Curtis, B., Haase, J., Abrams, M., Crippen, R., Carabajal, C., 2011. ASTER Global Digital Elevation Model Version 2 – Summary of Validation Results. NASA Land Processes Distributed Active Archive Center and the Joint Japan-US ASTER Science Team.

Takaku, J., Tadano, T., 2009. PRISM on-orbit geometric calibration and DSM performance. IEEE Trans. Geosci. Remote Sens. 47, 4060–4073. http://dx.doi.org/10.1109/TGRS.2009.2021649.

Tshering, P., Fujita, K., 2016. First in situ record of decadal glacier mass balance (2003–2014) from the Bhutan Himalaya. Ann. Glaciol. 57 (71), 289–294. http://dx.doi.org/10.3189/2016AoG71A036.

Venables, W.N., Ripley, B.D., 2002. Modern Applied Statistics with S. Springer, New York.

Yao, T., Thompson, L., Yang, W., Yu, W., Goa, Y., Guo, X., Yang, X., Duan, K., Zhao, H., Xu, B., Pu, J., Lu, A., Xiang, Y., Kattel, D.B., Joswiak, D., 2012. Different glacier status with atmospheric circulations in Tibetan Plateau and surroundings. Nat. Clim. Change 2, 663–667. http://dx.doi.org/10.1038/nclimate1580.

Zemp, M., Frey, H., Gärtner-Roer, I., Nussbaumer, S.U., Hoelzle, M., Paul, F., Haeberli, W., Denzinger, F., Ahlstrøm, A.P., Anderson, B., Bajracharya, S., Baroni, C., Braun, L.N., Cáceres, B.E., Casassa, G., Cobos, G., Dávila, L.R., Delgado Granados, H., Demuth, M.N., Espizua, L., Fischer, A., Fujita, K., Gadek, B., Ghazanfar, A., Hagen, J.O., Holmlund, P., Karimi, N., Li, Z.Q., Pelto, M., Pitte, P., Popovnin, V.V., Portocarrero, C.A., Prinz, R., Sangewar, C.V., Severskiy, I., Sigurðsson, O., Soruco, A., Usubaliev, R., Vincent, C., 2015. Historically unprecedented global glacier decline in the early 21st century. J. Glaciol. 61, 745–761. http://dx.doi.org/10.3189/2015JoG15J017.